



Article

Bone Regeneration by Dedifferentiated Fat Cells Using Composite Sponge of Alfa-Tricalcium Phosphate and Gelatin in a Rat Calvarial Defect Model

Nobuhito Tsumano ¹, Hirohito Kubo ², Rie Imataki ³, Yoshitomo Honda ⁴ , Yoshiya Hashimoto ^{5,*}  and Masahiro Nakajima ²

- ¹ Department of Oral and Maxillofacial Surgery, Graduate School of Dentistry, Osaka Dental University, 8-1, Kuzuha-hanazono-cho, Hirakata City 573-1121, Japan; tsumano@cc.osaka-dent.ac.jp
- ² Second Department of Oral and Maxillofacial Surgery, Osaka Dental University, 1-5-17, Otemae, Chuo-ku, Osaka 540-0008, Japan; kubo-h@cc.osaka-dent.ac.jp (H.K.); masa-na@cc.osaka-dent.ac.jp (M.N.)
- ³ Department of Pediatric Dentistry, Osaka Dental University, 1-5-17, Otemae, Chuo-ku, Osaka 540-0008, Japan; imataki-r@cc.osaka-dent.ac.jp
- ⁴ Department of Oral Anatomy, Osaka Dental University, 8-1, Kuzuha-hanazono-cho, Hirakata City 573-1121, Japan; honda-y@cc.osaka-dent.ac.jp
- ⁵ Department of Biomaterials, Osaka Dental University, 8-1, Kuzuha-hanazono-cho, Hirakata City 573-1121, Japan
- * Correspondence: yoshiya@cc.osaka-dent.ac.jp; Tel.: +81-906-066-7252



Citation: Tsumano, N.; Kubo, H.; Imataki, R.; Honda, Y.; Hashimoto, Y.; Nakajima, M. Bone Regeneration by Dedifferentiated Fat Cells Using Composite Sponge of Alfa-Tricalcium Phosphate and Gelatin in a Rat Calvarial Defect Model. *Appl. Sci.* **2021**, *11*, 11941. <https://doi.org/10.3390/app112411941>

Academic Editor: Gianrico Spagnuolo

Received: 5 November 2021

Accepted: 13 December 2021

Published: 15 December 2021

Publisher's Note: MDPI stays neutral with regard to jurisdictional claims in published maps and institutional affiliations.



Copyright: © 2021 by the authors. Licensee MDPI, Basel, Switzerland. This article is an open access article distributed under the terms and conditions of the Creative Commons Attribution (CC BY) license (<https://creativecommons.org/licenses/by/4.0/>).

Abstract: Mechanical and resorbable scaffolds are in high demand for stem cell-based regenerative medicine, to treat refractory bone defects in craniofacial abnormalities and injuries. Multipotent progenitor cells, such as dedifferentiated fat (DFAT) cells, are prospective sources for regenerative therapies. Herein, we aimed to demonstrate that a composite gelatin sponge (α -TCP/GS) of alfa-tricalcium phosphate (α -TCP) mixed with gelatin scaffolds (GS), with/without DFATs, induced bone regeneration in a rat calvarial defect model in vivo. α -TCP/GS was prepared by mixing α -TCP and 2% GS using vacuum-heated methods. α -TCP/GS samples with/without DFATs were transplanted into the model. After 4 weeks of implantation, the samples were subjected to micro-computed tomography (μ -CT) and histological analysis. α -TCP/GS possessed adequate mechanical strength; α -TCP did not convert to hydroxyapatite upon contact with water, as determined by X-ray diffraction. Moreover, stable α -TCP/GS was formed by electrostatic interactions, and verified based on the infrared peak shifts. μ -CT analyses showed that bone formation was higher in the α -TCP/GS+DFAT group than in the α -TCP/GS group. Therefore, the implantation of α -TCP/GS comprising DFAT cells enhanced bone regeneration and vascularization, demonstrating the potential for healing critical-sized bone defects.

Keywords: bone regeneration; alfa-tricalcium phosphate; animal study; dedifferentiated fat cells; rat calvarial defect

1. Introduction

Bone tissue reconstruction is often required in the maxillofacial region for mandibular defects resulting from cystectomy or highly atrophied alveolar bone. Autologous bone grafting is currently the most widely used bone reconstruction method for such cases [1]. However, autologous bone collection requires the invasion of normal tissues in addition to being subject to limits on the collection site and amount [2]. Filling bone defects with special composite biomaterials or tissue-engineered bone improves the bone-forming effect [3–5].

There are numerous studies on the combination of biopolymers and bioceramic-based composite scaffolds with improved mechanical and bone regeneration capabilities. Gelatin biopolymer is obtained from collagen through alkaline or acidic pre-treatment and thermal denaturation [6]. It is widely used for bone tissue regeneration, as it has a similar

composition as collagen, which accounts for approximately 95% of the organic phase of bone [7,8]. In addition, unlike collagen, gelatin is a modified biopolymer; the choice of gelatin as a scaffold material therefore precludes the immunogenicity and pathogen infection concerns associated with collagen [8]. However, the application of biopolymers to hard tissue regeneration scaffolds is limited because of the low mechanical strength of the latter. Researchers have developed hybrid scaffolds with combined biopolymers and bioceramics to enhance their mechanical properties [2,4,5,9,10]. Previous studies have demonstrated the role of alfa-tricalcium phosphate (α -TCP) particles in bone rebuilding by the gradual biodegradation and formation of adjacent bone [11,12]. Our previous studies [2,5] reported that transplantation of scaffolding material, made using porous α -TCP particles and chemically synthesized collagen model polypeptides, resulted in bone regeneration in beagle and mini pig bone defect models.

Although tissue engineering involves several types of cells, mesenchymal stem cells (MSCs), in particular, display therapeutic properties. MSCs from adipose tissue, also known as adipose-derived stem cells (ASCs), are extensively used for bone tissue engineering [13,14]. However, they are a heterogeneous cell population, particularly in the early passages; this may be attributed to their development from the non-adipocyte fraction of adipose tissue, such as the stromal vascular fraction [15]. Mature adipocytes isolated from fat tissue can be dedifferentiated into fibroblast-like cells by ceiling culture, and are referred to as dedifferentiated fat (DFAT) cells [16]. Our previous study [17] demonstrated that human DFAT cells have a higher ability to differentiate osteoblasts than ASC's DFAT cells from the human buccal fat pad.

The technical details regarding the use of DFAT cells for bone defect regeneration are unknown. The success rate of bone regeneration depends on the interaction between DFAT cells and the scaffold that holds and supports them. Gelatin and α -TCP are novel choices for preparing these scaffolds; whereas gelatin has natural pores to hold cells, α -TCP can provide suitable ions for stem cell growth. Therefore, we aimed to prepare allogeneic DFAT cells combined with α -TCP/gelatin scaffolds (GS) and implant them into rat calvarial defects, to examine their osteogenesis ability *in vivo*.

2. Materials and Methods

2.1. Preparation of Gelatin Sponge

Pig skin alkaline-treated gelatin (200 mg; LS-W, lotno. 210106, Nitta Gelatin, Osaka, Japan) was mixed in 10 mL of Milli-Q water at 65 °C for 1 h. After dissolving the gelatin at 65 °C, it was poured into Teflon plates and stored at 4 °C for 2 h prior to mixing with α -TCP. At that temperature, gelatin is in a gel state, and was confirmed to be gelatinized after 2 h. Subsequently, we prepared α -TCP (diameter of 500 μ m) solutions of 120 mg, 60 mg, or 30 mg per 120 μ L using a pipette tip. We then prepared α -TCP (diameter of 500 μ m) solutions of 120, 60, and 30 mg; the samples were stored at -80 °C for 24 h. The plate was lyophilized for 3 days with a DC800 lyophilizer (Yamato Co., Ltd., Tokyo, Japan) and thermally cross-linked using an ETTAS AVO-250NS vacuum dryer (AS ONE, Osaka, Japan), with a gauge pressure of -0.1 MPa at 150 °C for 24 h. The prepared complex was subjected to dry heat sterilization (160 °C, 8 h) before use. Figure 1 presents a cross-sectional view of the α -TCP/GS composite; α -TCP was uniformly present from the top to the bottom layers. [Figure 2] As the 120 mg α -TCP/GS composite collapsed when grasped with tweezers during transplantation (because of the numerous α -TCP granules), the 60 mg α -TCP/GS was selected to perform the analysis, including during *in vivo* testing.

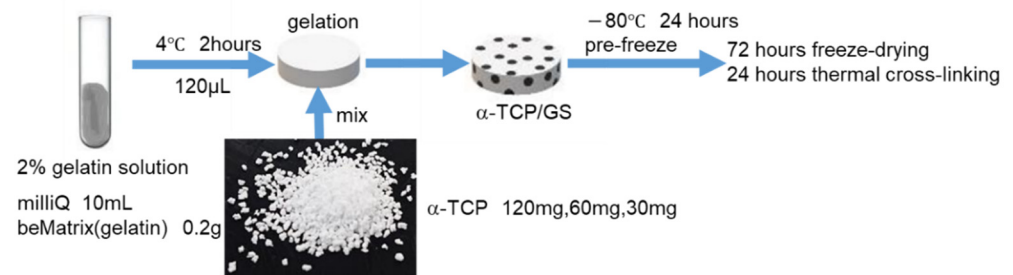


Figure 1. Fabrication method of α -TCP/GS.

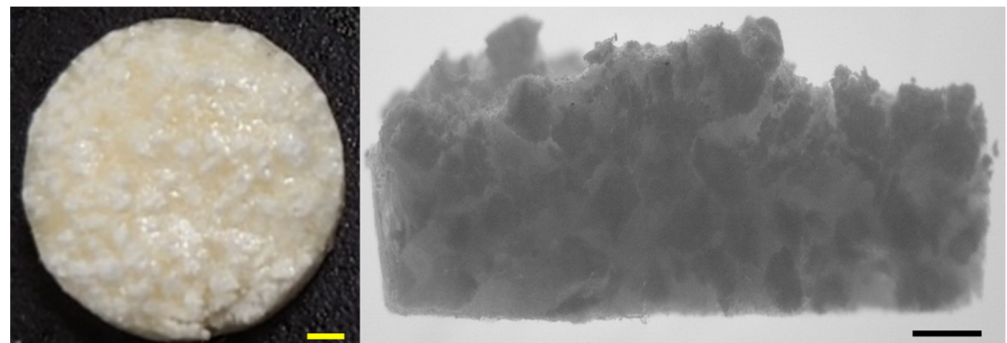


Figure 2. External and cross-sectional view of α -TCP/GS, composite gelatin sponge. Scale bar is 1.0 mm.

2.2. Thermogravimetric and Differential Thermal Analysis

We performed thermogravimetric and differential thermal analyses (TG/DTA) using STA2500 (NETZSCH, Yokohama, Japan). Measurements were performed in the air at a heating rate of 10 $^{\circ}$ C/min, in a temperature range of 30–800 $^{\circ}$ C. For TG/DTA, the sample was crushed with a mortar and pestle after freezing in liquid nitrogen; this was followed by examination of 11.0 and 3 mg of GS and GS/TCP, respectively.

2.3. Compression Test

Cylindrical specimens ($n = 3$) measuring 5 mm in diameter and 7.5 mm in height were prepared in a silicon tube mold for compression tests, following the procedures outlined in ISO9917-1. We prepared 0, 30, 60, and 120 mg α -TCP-containing solutions in 120 μ L of 2% Bematrix solution, in a dry condition. The samples were tested using a universal testing machine (AGS-X, Shimadzu Co., Kyoto, Japan). The load cell was 500 N and crosshead speed was 1 mm/min [18].

2.4. Scanning Electron Microscopy, X-ray Diffraction, and Fourier Transform Infrared Spectroscopy Analysis

α -TCP/GS was incubated in Dulbecco's modified Eagle's medium (DMEM; Nacalai Tesque, Kyoto, Japan) (without fetal bovine serum; FBS) for 24 h. Dehydration was achieved by placing the tissue in graded alcohols (50 \rightarrow 60 \rightarrow 70 \rightarrow 80 \rightarrow 90 \rightarrow 99 \rightarrow 100%) for 10 min each; this was followed by osmium coating. The samples were photographed using a scanning electron microscope (SEM; S-4800, Tokyo, Japan). Analysis using a powder X-ray diffractometer (XRD-6100) (Shimadzu Corporation, Kyoto, Japan) confirmed no change in the properties of α -TCP, before and after composite preparation. We also analyzed the properties of gelatin sponge and α -TCP alone, and in complex, by Fourier transform infrared spectroscopy (FTIR) (Spectrum One, Perkin-Elmer Inc., Waltham, MA, USA) with 16 scans at a 4 cm^{-1} resolution.

2.5. Fatty Tissue Collection

Animal experiments were performed in strict accordance with the guidelines approved by the Ethics Committee of the Osaka Dental College (approval number: 21-01002,

approved on 9 February 2021). Eight-week-old male F344 rats (250–280 g body weight) were purchased from Shimizu Laboratory Supply Co. (Kyoto, Japan), and were acclimated to the rearing environment for 1 week. The rats were then anesthetized with a triple mixture of anesthetics. The anesthetic mixture included midazolam (2 mg/kg; Midazolam Sandoz, Sandoz K.K., Yamagata, Japan), medetomidine hydrochloride (0.15 mg/kg; Medetomidine Hydrochloride 0.15 mg/kg; Domitor, Zenoac, Fukushima, Japan), and butorphanol tartrate (2.5 mg/kg; Vetorphale, MeijiSikaParma Co., Ltd., Tokyo, Japan). Rats received 0.2 mL of anesthetics per 100 mg of body weight. The inguinal area was shaved and disinfected, the skin over the inguinal area was incised, and fat was bluntly removed. Approximately 1 g of white fat was collected, and the rats were euthanized by overdosing with pentobarbital [19].

2.6. Isolation and Culture of Rat DFATs

Rat DFAT was isolated using the ceiling culture method. The adipocytes were lysed and minced with 0.1% collagenase type I (Fujifilm Wako Pure Chemical Co., Ltd., Osaka, Japan) by stirring slowly at 37 °C for 1 h, and the cell suspension was filtered through 150 µm and 250 µm nylon meshes. The adipocytes were then allowed to pass through, whereas unwanted stromal cells and tissues were removed. We collected the mature adipocytes floating on the top layer, and centrifuged them at 1000 rpm for 3 min at 4 °C. We then collected 200 µL liquid from the separated mature adipocyte layer, and placed them in 25 cm² culture flasks (Thermo Fisher Scientific Inc., Waltham, MA, USA) filled with DMEM, supplemented with 20% FBS (lot number AE24573269 HyClone). An antibiotic/antifungal mixture stock solution consisting of 10,000 U/mL penicillin, 10,000 µg/mL streptomycin, and 25 µg/mL amphotericin B (Nacalai Tesque) was added to the DMEM containing 20% FBS. The cells were incubated in 5% CO₂ at 37 °C, followed by the addition of a mixed stock solution. The flasks were left with the adherent culture surface, such that the floating adipocytes containing lipid droplets adhered to the inner surface of the flask ceiling. One week later, the flasks were inverted and replaced with 5 mL of DMEM, containing 10% FBS; the medium was changed twice weekly. The cells were passaged when confluent, and passage 2 of the DFATs was used in all experiments. We used this procedure for obtaining DFAT cells and characterized them with CD markers, to verify the accuracy of the cell population [19] [Figure 3].

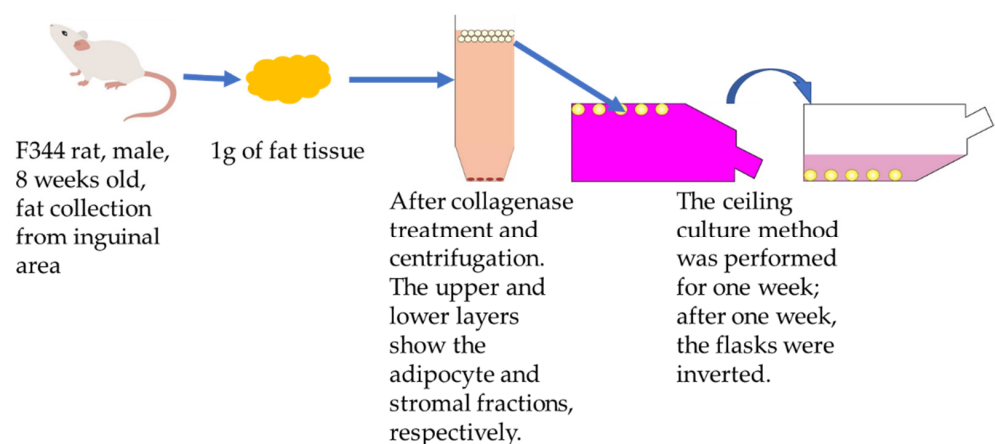


Figure 3. Procedure for creating DFAT cells.

2.7. Cell Seeding into the Scaffold and Scanning Electron Microscopy Analysis and DAPI Staining

The prepared DFAT was cultured in a normal medium, and approximately 2.0×10^6 /cells were recovered. Thereafter, we prepared and seeded a 50 µL suspension with 2.0×10^6 /cells in a complex, placed on a 12-well plate with 2 mL FBS-free DMEM. The cells were then incubated at 37 °C in 5% CO₂ for 1 day. Cell Count Reagent SF (07553-44 Nacalai, Kyoto, Japan) was added to the GS and α-TCP/GS, at the concentration mentioned in the accompanying document. The cells were incubated for 3 h after the addition of the reagent,

and the absorbance at 450 nm was measured using a plate reader. The samples were washed with Dulbecco's phosphate-buffered saline (D-PBS) (-), and the cells were fixed in 4% paraformaldehyde solution and warmed to 37 °C for 24 h. After washing twice with D-PBS (-), the cells were dehydrated in graded alcohol of 50–100% ethanol. The solution was treated with isoamyl acetate solution for 24 h, and dried using a critical point dryer; the sample was also photographed using a SEM (S-4800, Tokyo, Japan). Paraffin embedding was performed and thin sections were made, and sealed with DAPI-Fluoromount-G (0100-20, Southern Biotechnology Associates, Birmingham, UK). The cells were observed with a fluorescence microscope (BZ-9000).

2.8. Surgery

Male 8-week-old F344 rats were used for the transplantation experiments. A critical sized defect (diameter: 9 mm) was implanted in the center of the rat calvaria using a trephine bar (Dentech, Tokyo, Japan), and the defects were filled using α -TCP/GS; the control group (defect group) was only administered saline. The rats were divided into the following groups: 1 = defect group, 2 = GS group, group 3 = GS + DFAT group, 4 = α -TCP/GS group, and 5 = α -TCP/GS + DFAT group. A total of 20 rats were used in the experiment (4 rats \times 5 groups). Four weeks' post-transplantation, the rats in each group were euthanized by overdosing with pentobarbital. The calvaria of each group were collected, and all samples were fixed in a 4% phosphate buffered paraformaldehyde solution (Fujifilm Wako Pure Chemical Industries, Ltd., Osaka, Japan) for 24 h. Following fixation for 24 h, we performed μ -CT.

2.9. Bone Morphometric Analysis

Four weeks after transplantation, the rats were euthanized and the calvaria were incised; bone regeneration status was evaluated with μ -CT (SKYSCAN 1275; Bruker, Billerica, MA, USA). The settings for sample measurement were as follows: source voltage (kV) = 65, source current (μ A) = 85, and pixel size (μ m) = 30 and 1 mm aluminum filter. Automatic air calibration was performed. We reconstructed the axial bone mineral density (BMD) images of the samples using a three-dimensional (3-D) image analysis system (CTAn/Bruker, Billerica, MA, USA). Bone formation was measured as the radiopacity volume/total volume (RV/TV).

2.10. Histological Assessment

Following μ -CT, the treated area was sectioned coronally through the midline. The split anterior section was washed thrice with D-PBS (-), and the washed tissue was embedded in SCEM (SECTION-LAB Co., Ltd., Hiroshima, Japan) and stored at -80 °C. Before staining, the tissue was sectioned in 7 μ m slices and stained with von Willebrand factor (vWF/Factor VIII). New vessels (α -TCP/GS, α -TCP/GS + DFAT) in four tissue sections from each of the four rats were counted for evaluating neovascularization, using ImageJ (Wayne Rasband, National Institutes of Health, Bethesda, MD, USA). In contrast, we decalcified the divided posterior half using Decalcifying Solution B (041-22031, FUJIFILM Wako Pure Chemical Corporation, Osaka, Japan) for 4 weeks. The demineralization solution was changed once per week at 4 °C, with stirring. Following demineralization, we prepared paraffin blocks, and the treated area was sectioned coronally. The paraffin blocks were faced to include the entire treated area, and these blocks were cut into 3 μ m pieces and stained with hematoxylin and eosin (HE).

2.11. Statistical Analysis

Data were evaluated using the one-way analysis of variance, followed by the Bonferroni and Student's t-tests (BellCurve for Excel, Tokyo, Japan).

3. Results

3.1. TG/DTA

We performed thermal analysis of GS and GS/TCP using TG/DTA; the thermal degradation of GS occurred in two stages. The first stage occurred at a temperature of 30–90 °C, because of the loss of water molecules. The second stage comprised the primary degradation of gelatin at 237 °C; the gelatin was completely degraded at approximately 590 °C. A sharp temperature peak was observed at 592 °C. From the GS/TCP profile, the first weight loss was observed between 260 and 400 °C due to the evaporation of absorbed water, and the second moderate weight loss was observed until 550 °C due to the thermal decomposition of gelatin; however, there was no significant change at high temperatures (Figure 4).

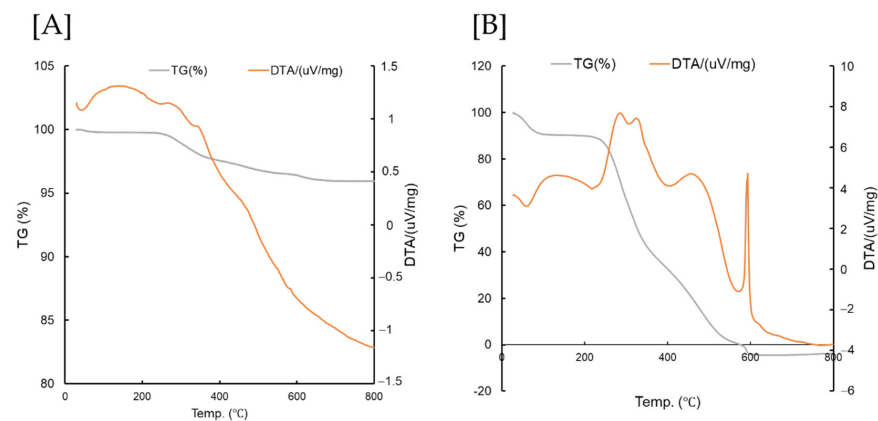


Figure 4. TG/DTA of α -TCP/GS (A) and GS (B); TG/DTA, thermogravimetric and differential thermal analyses; α -TCP/GS, composite gelatin sponge; and GS, gelatin scaffolds. The grey line represents the results of TGA and the orange line represents the results of DTA.

3.2. XRD

Figure 5 shows the peaks of only α -TCP and α -TCP/GS. The diffraction peaks of α -TCP/GS are reduced compared to those of the original α -TCP particles. However, a comparison of the XRD pattern of the synthesized α -TCP particles with the α -TCP data registered with the International Center for Diffraction Data (ICDD) confirms that these peaks appear at consistent angles.

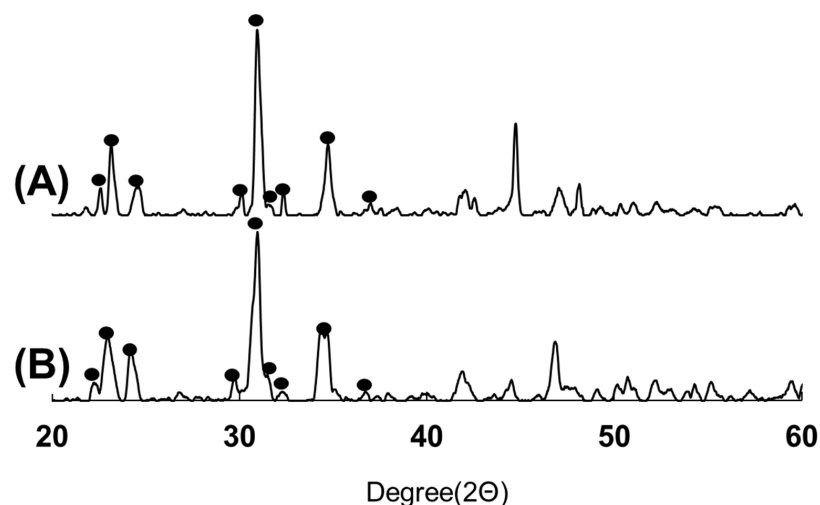


Figure 5. X-ray diffraction pattern of α -TCP/GS (A) and α -TCP particles (B); α -TCP/GS, composite gelatin sponge; α -TCP, alfa-tricalcium phosphate. The circles indicate the characteristic peaks of α -TCP.

3.3. FTIR

Figure 6 depicts the FTIR spectrum of α -TCP/GS. α -TCP peaks were observed at 582, 988, and 1022 cm^{-1} . We observed amide peaks at 1530 and 1231 cm^{-1} and a carboxyl peak at 1338 cm^{-1} in the spectrum for gelatin. Among these peaks, the one at 1631 cm^{-1} shifted to a higher wave number (1637 cm^{-1}) in α -TCP/GS (Figure 5).

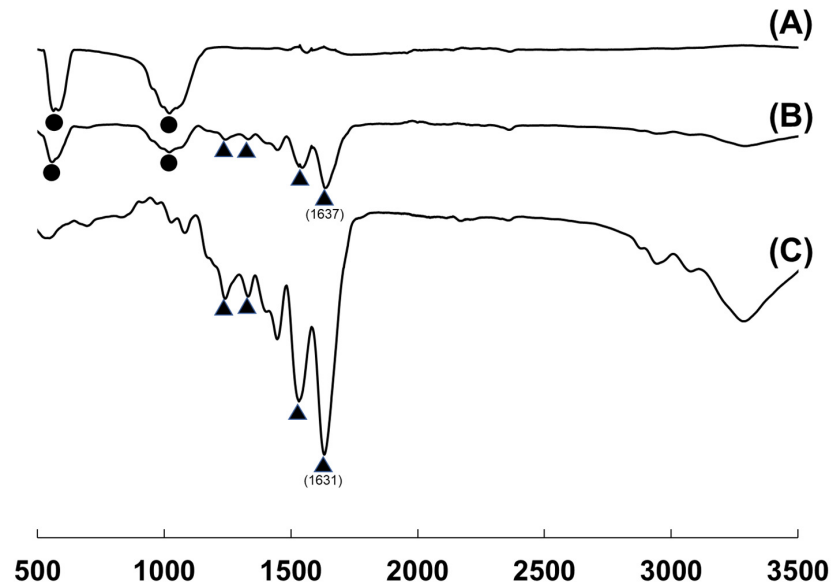


Figure 6. Results of FTIR. (A) α -TCP; (B) α -TCP/GS; and (C) GS. α -TCP/GS, composite gelatin sponge; GS, gelatin scaffolds; and α -TCP, alfa-tricalcium phosphate. The circles represent the characteristic peaks of α -TCP, whereas the triangles represent those of gelatin.

3.4. Compression Test

The maximum compressive stress in the groups containing 120 and 60 mg of α TCP in 2% gelatin solution was 0.53 and 0.45 MPa, respectively. Conversely, the stress was low in the group containing 30 mg of α TCP (Figure 7). Based on the results of this experiment, we decided that all α -TCP/GS composites used in other experiments, including the transplantation experiment, should contain 60 mg of α -TCP.

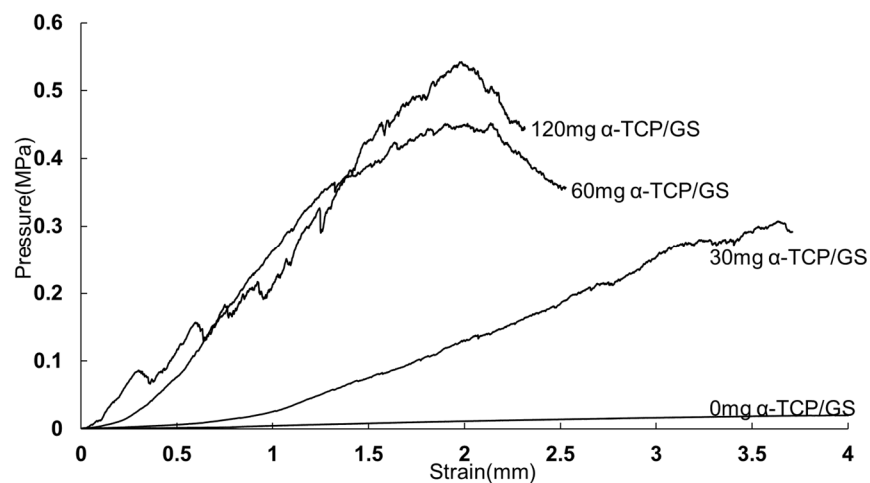


Figure 7. Results of the compression test. The vertical axis represents pressure (unit: MPa). The horizontal axis represents the elapsed time (unit: mm) since detection of compression stress.

3.5. SEM of Synthesized Material

Figure 8 presents an SEM image of the synthesized porous ceramic particles; the particles displayed a continuous pore structure with a pore diameter of approximately 5–50 μm . The α -TCP/GS was composed of α -TCP particles, and a 3-D porous structure and a gelatin sponge was observed in the form of a sheet.

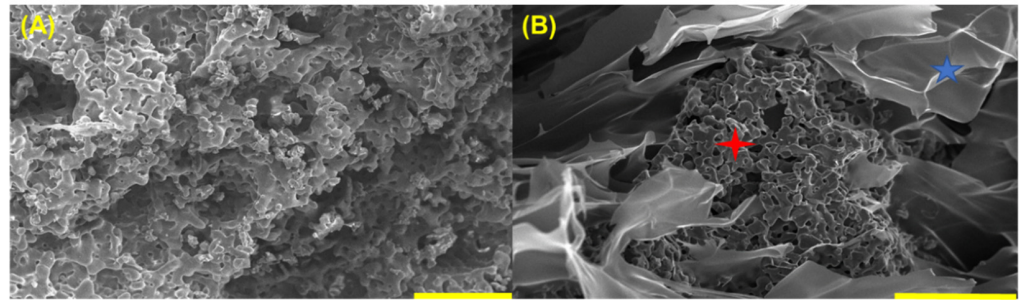


Figure 8. SEM image of the material (A) α -TCP and (B) α -TCP/GS. The red cross indicates α -TCP, and the blue star indicates gelatin sponge. The yellow scale bar represents a length of 50 μm .

3.6. The Cell Numbers of GS and α -TCP/GS 24 h after DFAT Seeding

The cell numbers of GS and α -TCP/GS were 4.4×10^6 and 3.4×10^6 , respectively (Figure 9).

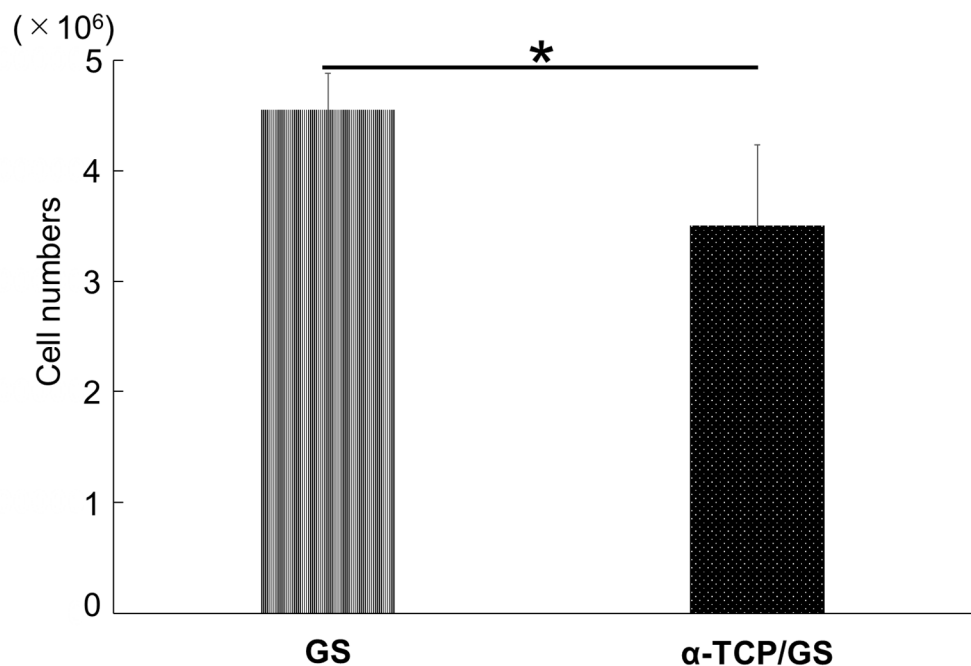


Figure 9. The cell numbers of GS and α -TCP/GS, 24 h after DFAT seeding. Student's *t*-test; * $p < 0.05$; $n = 4$.

3.7. SEM after DFAT Seeding and DAPI Staining

Figure 10 depicts the cell attachment behavior of DFATs on α -TCP/GS. Several cells attached to α -TCP; some cells displayed a spreading morphology, a characteristic form of DFAT. Figure 11 is an image of DFAT seeded on α -TCP/GS and DAPI stained; the cell nuclei of DFAT are stained in the center of α -TCP/GS.

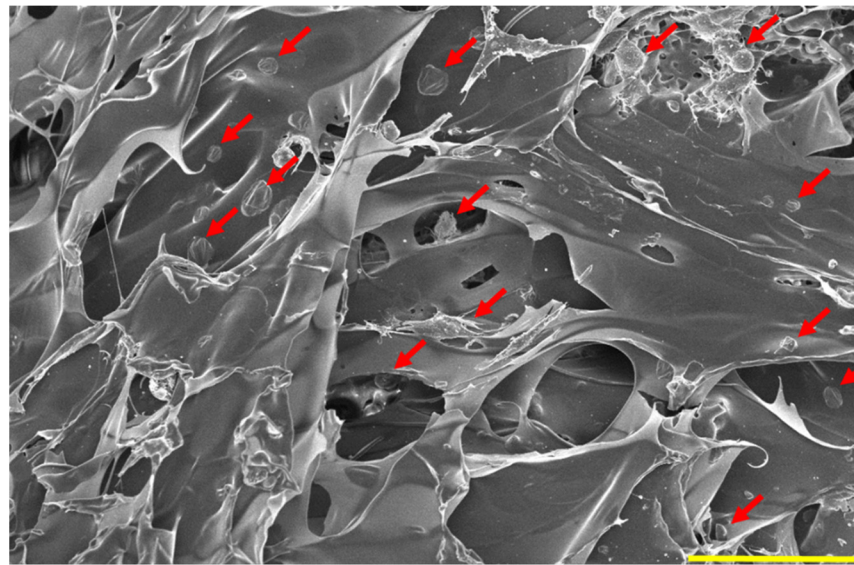


Figure 10. DFATs attachment property of α -TCP/GS. DFATs, dedifferentiated fat cells; α -TCP/GS, composite gelatin sponge. The red arrows indicate DFAT. The yellow scale bar represents a length of 50 μm .

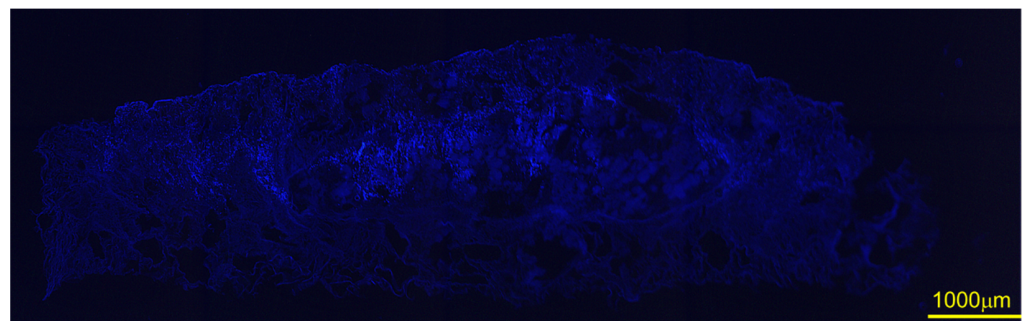


Figure 11. Images of DFAT seeded on α -TCP/GS and stained with DAPI. Scale bar is in 1000 μm .

3.8. Bone Morphometric Analysis

Figure 11 shows the reconstructed CT images. Although small bone was found in the defect, sponge, and GS groups, it was insufficient to be considered bone regeneration (Figure 12A–C). The α -TCP/GS group showed considerable residual α -TCP (Figure 12D); the α -TCP/GS + DFAT group showed bone regeneration from the edge of the defect (Figure 12E). Figure 12 presents μ -CT 3-D reconstructed images and the BMD distribution map. Each experimental group was analyzed at 4 weeks' post-surgery; the BMD of each group is displayed in the 3-D map. High, middle, and low BMD are indicated on the color scale by blue and green, orange and yellow, and red and purple. Lesser bone regeneration was observed in the bone defect group; similarly, bone regeneration was rarely observed in the GS and the GS + DFAT (Figure 13A–C) groups. Several α -TCP granules persisted, with moderate new bone being observed at the edge of the defect (Figure 13D). In the α -TCP/GS+ DFAT group, new bone formed from the margin of the defect that displayed high BMD; the BMD value was similar to that of the mother bed bone. In addition, BMD images demonstrated that the α -TCP granules were bound to the adjacent α -TCP granules and resorbed (Figure 13E).

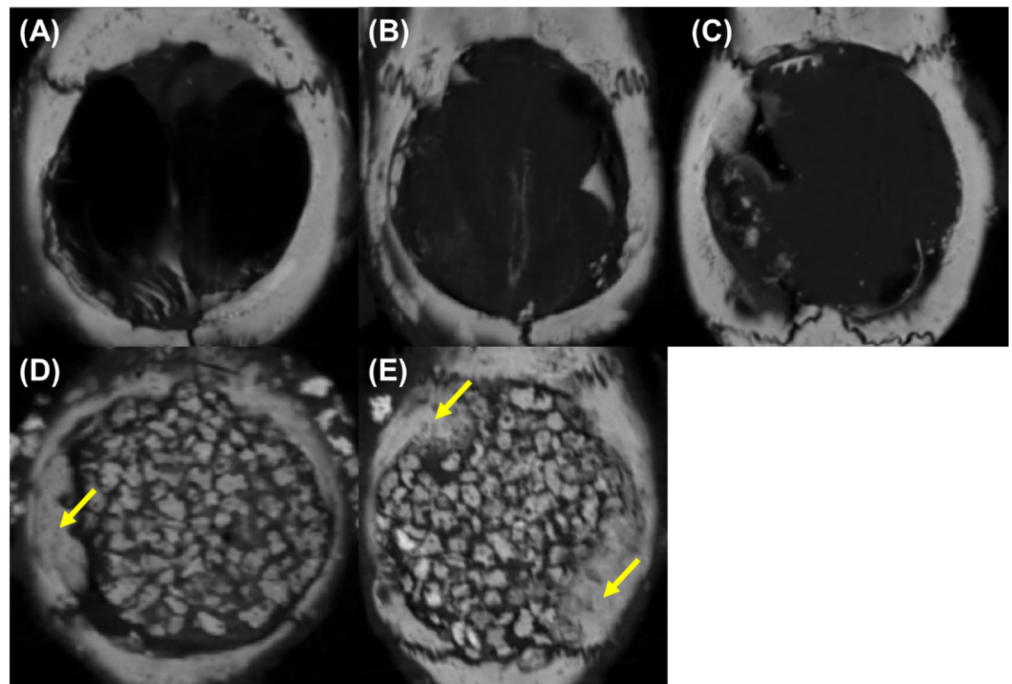


Figure 12. Reconstructed image of CT (A) defect group, (B) GS group, (C) GS + DFAT group, (D) α -TCP/GS group, and (E) α -TCP/GS + DFAT group α -TCP/GS, composite gelatin sponge; GS, gelatin scaffolds; and DFAT, dedifferentiated fat cell. The yellow arrows indicate to new bone.

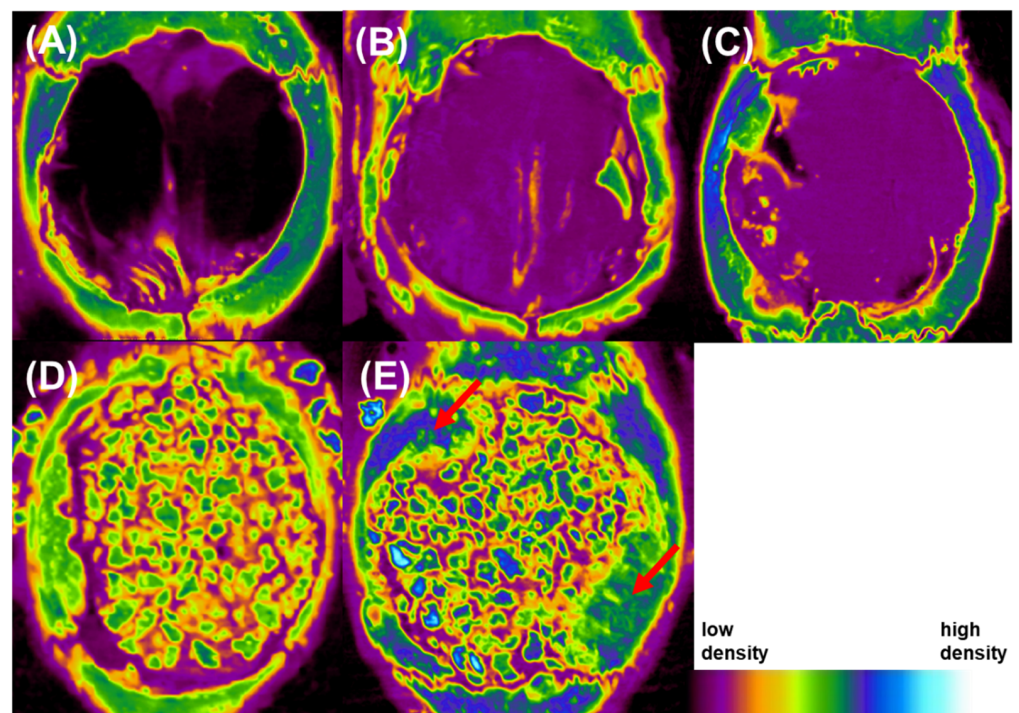


Figure 13. BMD images (A) defect group, (B) GS group, (C) GS + DFAT group, (D) α -TCP/GS group, and (E) α -TCP/GS + DFAT group BMD, bone mineral density; α -TCP/GS, composite gelatin sponge; GS, gelatin scaffolds; and DFAT, dedifferentiated fat cell. The red arrows indicate new bone.

We performed quantitative image analysis of newly developed bone (Figure 14). There were no significant differences in RV/TV between the defect only, GS, and GS + DFAT. α -TCP/GS + DFAT demonstrated 56.95% RV/TV, which was the highest in the groups tested.

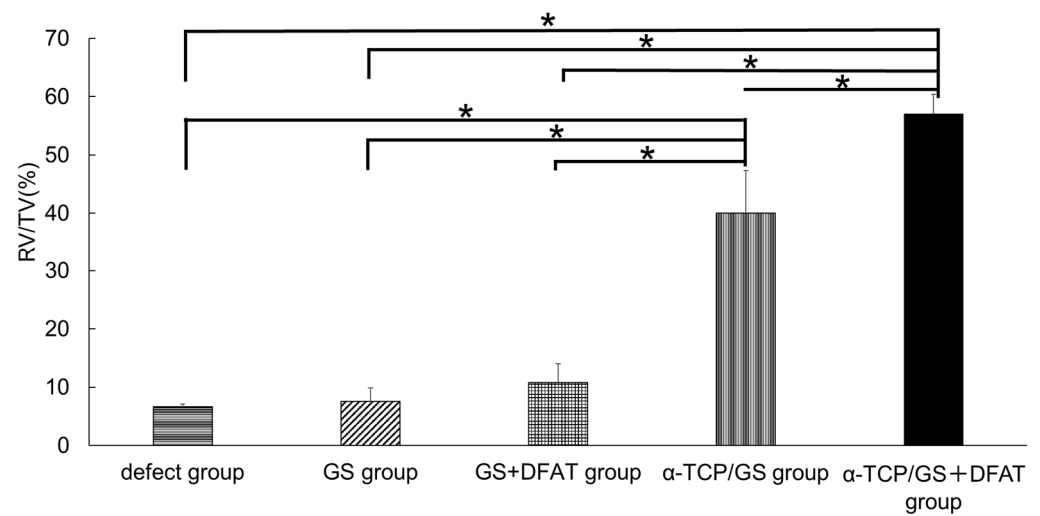


Figure 14. Results of μ -CT analysis of bone mass μ -CT, micro-computed tomography; RV, radiopacity volume; and TV, total volume. Bonferroni test; * $p < 0.05$; $n = 4$.

3.9. Hematoxylin and Eosin Stain

Figure 15 depicts the HE-stained images. In the defect alone group, we observed callus in a part of the bone defect; however, most of it was occupied by fibrous connective tissue. The sponge alone group comprised denser fibrous connective tissue than the defect alone group with some bone structures. In the α -TCP/GS group, α -TCP granules remained and were not replaced with bone; several bone tissues were immature. The α -TCP/GS + DFAT group comprised more new bones than the α -TCP/GS group, although slight absorption of α -TCP granules was observed. In addition, we identified the formation of osteoids around the α -TCP granules.

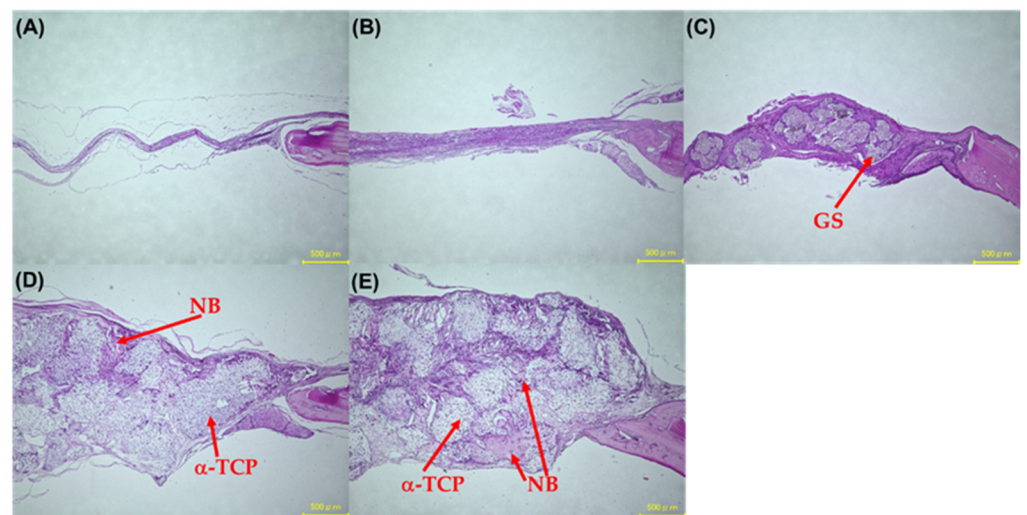


Figure 15. HE stained tissue specimen (A) defect group, (B) GS group, (C) GS + DFAT group, (D) α -TCP/GS group, and (E) α -TCP/GS + DFAT group. α -TCP/GS, composite gelatin sponge; GS, gelatin scaffolds; and DFAT, dedifferentiated fat cell. Scale bar indicates 500 μ m. NB: new bone; GS: gelatin sponge.

3.10. Immunohistochemical Evaluation

Figure 16 depicts an immunostaining image of vWF (Factor VIII). The GS/TCP group (Figure 16A) displayed new blood vessels in the tissue. In contrast, new blood vessels were observed around the α -TCP granules in the α -TCP/GS + DFAT group, as indicated by the arrows (Figure 16B). The number of new vessels was counted by Image J; the number of new vessels in α -TCP/GS + DFAT was significantly higher than in α -TCP/GS (Figure 17).

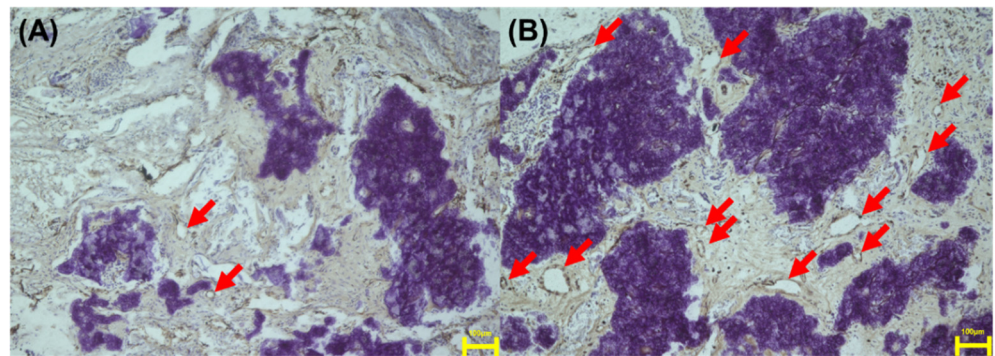


Figure 16. Tissue specimen of immunostaining (Factor VIII). (A) α -TCP/GS group and (B) α -TCP/GS + DFAT group. α -TCP/GS, composite gelatin sponge; GS, gelatin scaffolds; and DFAT, dedifferentiated fat cell. Arrows indicate blood vessels. The scale bar represents a length of 100 μ m.

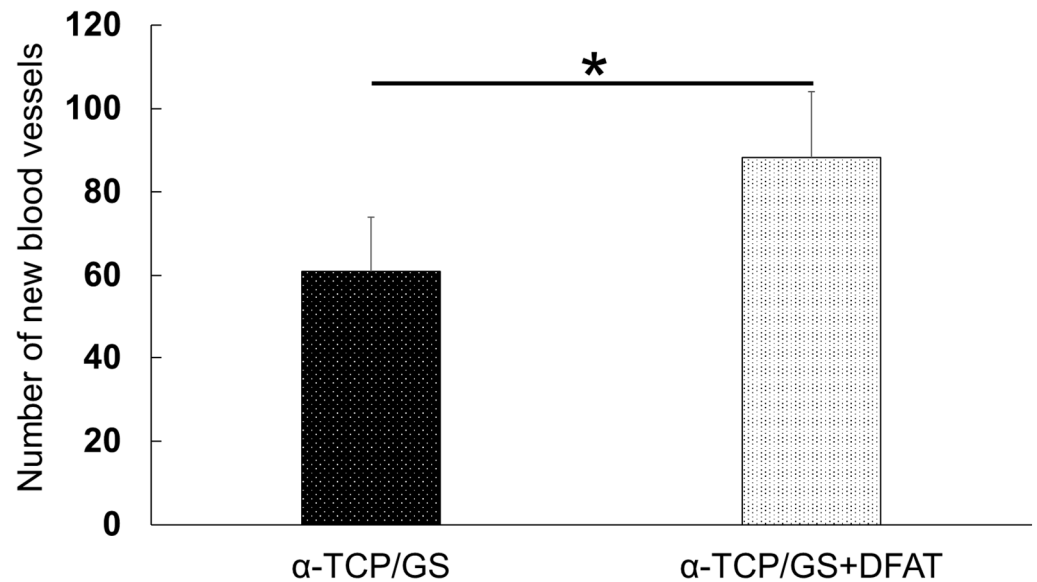


Figure 17. Results of the analysis of the number of new blood vessels; Student's *t*-test; * $p < 0.05$; $n = 4$.

4. Discussion

The cells that form the regenerating tissue, including mature, progenitor, and stem cells, play an important role in the success of tissue regeneration. Numerous studies have evaluated MSCs combined with scaffolds for inducing *in vitro* or *in vivo* tissue regeneration. Gelatin is a natural polymer derived from partially hydrolyzed collagen [20,21]. Our previous study using gelatin sponge for bone regeneration indicated the value of using rat DFATs in conjunction with a platelet-rich plasma [19]. In addition, gelatin chemically modified with epigallocatechin gallate in combination with DFATs can facilitate the induction of bone regeneration [22]. However, the application of gelatin to hard tissue regeneration scaffolds is limited, due to the low mechanical strength of the latter. We studied the *in vivo* bone healing potential of DFAT-loaded α -TCP/gelatin sponge, transplanted into an athymic critical-sized rat calvarial defect model.

In our previous study [19], GS was fabricated using a 1% gelatin solution. The combination of α -TCP particles with 1% gelatin solution precipitated α -TCP particles at the bottom of the solution; this may be attributed to their sol state at 4 °C. Therefore, we used a 2% gelatin solution in the gel state. Although the strength of the composite sponge is likely to increase with the number of α -TCP granules added to the gelatin, adding excess α -TCP granules makes it fragile and impairs the ability to form a composite sponge. The 120 mg α -TCP/GS composite displayed a mechanical strength similar to that of 60 mg

α -TCP/GS; however, it collapsed when grasped with tweezers because of the numerous α -TCP granules. In addition to sufficient mechanical strength, the operability for grafting is an important requirement for bone defect graft materials.

The high-temperature peak of the GS sponge in the TGA profile was higher than that in our previous study [19], because of a change in the gelatin concentration from 1% to 2%. In the TGA profile of the α -TCP/GS sponge, there was no significant weight loss at high temperatures (above 600 °C); this could be explained by use of 60 mg α -TCP/GS (96.2 wt% of α -TCP content). Yilmaz et al. [23] revealed that there is no significant change in the weight of hydroxyapatite even at high temperatures. Our findings indicated that α -TCP maintained its thermal stability.

We prepared a composite sponge by mixing gelatin and porous α -TCP. The ceramic body comprised a continuous pore structure with a pore diameter of approximately 10–50 μ m, and a sponge-like scaffold with a grain size of 500 μ m. The porous body of TCP can gradually dissolve away from the bone defect during bone repair, and can be replaced by the regenerated bone. This microporous bioresorbable ceramic is useful as a bone filler for medical applications; this is because its porous structure facilitates cell invasion [24]. However, the solubility of porous α -TCP may be higher than that of the original α -TCP; thus, it is more likely to be completely absorbed by the body before bone regeneration can repair the defect [2]. In this study, a mixture of porous α -TCP and gelatin was effective for controlling the degradation rate of the implanted α -TCP.

In addition, there was no significant difference between the XRD patterns of α -TCP/GS and α -TCP. The absence of hydroxyapatite can be attributed to the freeze drying of TCP and gelatin scaffolds under reduced pressure immediately after mixing, which reduced the contact time with moisture. Moreover, the FTIR analysis did not reveal any significant change between α -TCP alone and the composite. The peak for GS (1631 cm^{-1}) slightly shifted to a higher wave number (1640 cm^{-1}) in the α -TCP/GS, due to the electrostatic interaction between calcium ions in α -TCP and carboxyl groups in gelatin [25,26].

In the present study, seeding was performed via droplet seeding; DFATs displayed a rounded appearance, and were evenly dispersed within the pores of the scaffolds 24 h post-seeding. The seeding of droplets and the subsequent static culture is associated with the concentration of cells around the scaffold, as air becomes trapped in the center of the porous scaffold [27,28]. In this experiment, the cell suspension volume was set at 50 μ L. When the volume of the cell suspension was 50 μ L, the cell numbers of GS and α -TCP/GS were 4.4×10^6 and 3.4×10^6 , respectively, 24 h after DFAT seeding.

Undifferentiated pluripotent progenitor cells for bone regeneration therapy are commonly used in vitro to differentiate osteoblasts using bone-forming medium, prior to cell transplantation. Yanagi et al. [29] demonstrated that no significant difference was noted in the BMD of three-dimensional spheroids DFAT transplantation with or without osteogenic stimulation into rat calvarial defects. In this study, DFATs were transplanted in vitro without osteoblast induction, considering the cost issues of future clinical applications. However, we identified remaining α -TCP and new bone surrounding the α -TCP on the CT and HE staining images of the α -TCP/DFATs group. Bone regeneration occurred upon DFAT transplantation into bone defects; Watanabe et al. [30] demonstrated that the therapeutic angiogenic effects of DFAT cells occurred due to secretion of angiogenic factors and pericyte differentiation by transforming growth factor β 1 signaling, via Smad2/3. The transplanted cells release a variety of factors that accelerate healing, thereby accelerating the healing of the bone defect, and causing bone formation. Angiogenesis during bone healing can be confirmed by immunohistochemistry staining for vWF, platelet endothelial cell adhesion molecule (CD31), and the pericyte marker alpha-smooth muscle actin (α -SMA) [31]. Newly formed vessels stained by factor VIII, which forms a complex with vWF, were prominent around the surface of α -TCP particles.

In conclusion, this study demonstrated that α -TCP granules and gelatin sponges possessed adequate mechanical strength. α -TCP did not convert to hydroxyapatite upon contact with water, and a stable α -TCP/GS composite was formed by electrostatic inter-

actions, which were verified based on their infrared peak shifts. Bone regeneration was promoted in the DFAT/ α -TCP/GS group by increasing the bone volume, as evidenced by μ -CT analyses. The transplantation of the α -TCP/GS comprising DFAT cells enhanced bone regeneration and vascularization, demonstrating its potential for healing critical-size bone defects. Among the groups studied in a rat calvarial defect model in this study, the group transplanted with α -TCP-GS with DFAT cells demonstrated greatest bone regeneration after 4 weeks of transplantation.

Author Contributions: N.T., H.K. and Y.H. (Yoshitomo Honda) conceived and designed the experiments; N.T., R.I. performed the experiments; N.T. analyzed the data; N.T. contributed reagents/materials/analysis tools; N.T., H.K., Y.H. (Yoshiya Hashimoto) and M.N. wrote the paper. All authors have read and agreed to the published version of the manuscript.

Funding: This work was supported in part by JSPS KAKENHI grant nos.17K11864 and 20K10195.

Institutional Review Board Statement: The animal experiments in this study strictly conformed to the guidelines approved by the local ethics committee of the Osaka Dental University (approval no. 21-01002, approved on 9 February 2021).

Acknowledgments: The authors acknowledge Mariko Nakai (Graduate School of Biomaterials, Osaka Dental University) for assisting with conceptualization, Zhang Ye (Graduate School of Biomaterials, Osaka Dental University) for her assistance with the animal experiments, and Kengo Iwasaki (Institute of Dental Research, Osaka Dental University) for his assistance during the study. The authors would also like to acknowledge the Bioscience Division of KAC Corporation, which performed pathological tissue preparation and staining, and Yasuyuki Kobayashi of the Osaka Research Institute of Industrial Science and Technology for TG/DTA analysis.

Conflicts of Interest: The authors declare no conflict of interest.

References

1. Cohen, M.; Polley, J.W.; Figueroa, A.A. Secondary (intermediate) alveolar bone grafting. *Clin. Plast. Surg.* **1993**, *20*, 691–705. [[CrossRef](#)]
2. Ito, T.; Hashimoto, Y.; Baba, S.; Iseki, T.; Morita, S. Bone regeneration with a collagen model polypeptides/ α -tricalcium phosphate sponge in a canine tibia defect model. *Implant Dent.* **2015**, *24*, 197–203. [[CrossRef](#)] [[PubMed](#)]
3. Baba, S.; Inoue, T.; Hashimoto, Y.; Kimura, D.; Ueda, M.; Sakai, K.; Matsumoto, N.; Hiwa, C.; Adachi, T.; Hojo, M. Effectiveness of scaffolds with pre-seeded mesenchymal stem cells in bone regeneration—assessment of osteogenic ability of scaffolds implanted under the periosteum of the cranial bone of rats. *Dent. Mater. J.* **2010**, *29*, 673–681. [[CrossRef](#)] [[PubMed](#)]
4. Matsuno, T.; Nakamura, T.; Kuremoto, K.I.; Notazawa, S.; Nakahara, T.; Hashimoto, Y.; Satoh, T.; Shimizu, Y. Development of β -tricalcium phosphate/collagen sponge composite for bone regeneration. *Dent. Mater. J.* **2006**, *25*, 138–144. [[CrossRef](#)]
5. Sakai, K.; Hashimoto, Y.; Baba, S.; Nishiura, A.; Matsumoto, N. Effects on bone regeneration when collagen model polypeptides are combined with various sizes of alpha-tricalcium phosphate particles. *Dent. Mater. J.* **2011**, *30*, 913–922. [[CrossRef](#)]
6. Kroschwitz, J.I. *Encyclopedia of Polymer Science and Engineering*; John Wiley & Sons, Inc.: Hoboken, NJ, USA, 2004.
7. Alvarez, K.; Nakajima, H. Metallic Scaffolds for Bone Regeneration. *Materials* **2009**, *2*, 790–832. [[CrossRef](#)]
8. Liu, X.; Smith, L.A.; Hu, J.; Ma, P.X. Biomimetic nanofibrous gelatin/apatite composite scaffolds for bone tissue engineering. *Biomaterials* **2009**, *30*, 2252–2258. [[CrossRef](#)]
9. Hashimoto, Y.; Adachi, S.; Matsuno, T.; Omata, K.; Yoshitaka, Y.; Ozeki, Y.; Umezu, Y.; Satoh, T.; Nakamura, M. Effect of an injectable 3D scaffold for osteoblast differentiation depends on bead size. *Biomed. Mater. Eng.* **2009**, *19*, 391–400. [[CrossRef](#)]
10. Matsuno, T.; Hashimoto, Y.; Adachi, S.; Ozeki, Y.; Umezu, Y.; Tabata, Y.; Nakamura, M.; Yamaguchi, Y.; Satoh, T. Preparation of injectable 3D-formed β -tricalcium phosphate beadalginate composite for bone tissue engineering. *Dent. Mater. J.* **2008**, *26*, 827–834. [[CrossRef](#)]
11. Handa, T.; Anada, T.; Honda, Y.; Yamazaki, H.; Kobayashi, K.; Kanda, N.; Kamakura, S.; Echigo, S.; Suzuki, O. The effect of an octacalcium phosphate co-precipitated gelatin composite on the repair of critical-sized rat calvarial defects. *Acta Biomater.* **2012**, *8*, 1190–1200. [[CrossRef](#)]
12. Hashimoto, Y.; Kaida, K.; Uemura, N.; Kimura, D.; Matsuse, K.; Ueda, M.; Hirose, M.; Toda, I.; Komuro, A.; Kawaue, Y.; et al. Bone Regeneration with a Collagen Model Polypeptideporous Alpha-tricalcium Phosphate Sponge. *J. Oral Tissue Engin* **2016**, *14*, 41–50.
13. Mizuno, H.; Tobita, M.; Uysal, A.C. Concise review Adipose-derived stem cells as a novel tool for future regenerative medicine. *Stem Cells* **2012**, *30*, 804–810. [[CrossRef](#)] [[PubMed](#)]

14. Yoon, E.; Dhar, S.; Chun, D.E.; Gharibjanian, N.A.; Evans, G.R. In vivo osteogenic potential of human adipose-derived stem cells/poly lactide-co-glycolic acid constructs for bone regeneration in a rat critical-sized calvarial defect model. *Tissue Eng.* **2007**, *13*, 619–627. [[CrossRef](#)] [[PubMed](#)]
15. Matsumoto, T.; Kano, K.; Kondo, D.; Fukuda, N.; Iribe, Y.; Tanaka, N.; Matsubara, Y.; Sakuma, T.; Satomi, A.; Otaki, M.; et al. Mature adipocyte-derived dedifferentiated fat cells exhibit multilineage potential. *J. Cell. Physiol.* **2008**, *215*, 210–222. [[CrossRef](#)] [[PubMed](#)]
16. Yagi, K.; Kondo, D.; Okazaki, Y.; Kano, K. A novel preadipocyte cell line established from mouse adult mature adipocytes. *Biochem. Biophys. Res. Commun.* **2004**, *321*, 967–974. [[CrossRef](#)]
17. Kishimoto, N.; Momota, Y.; Hashimoto, Y.; Tatsumi, S.; Ando, K.; Omasa, A.; Kotani, J. The osteoblastic differentiation ability of human dedifferentiated fat cells is higher than that of adipose stem cells from the buccal fat pad. *Clin. Oral Investig.* **2014**, *18*, 1893–1901. [[CrossRef](#)]
18. Imataki, R.; Shinonaga, Y.; Nishimura, T.; Abe, Y.; Arita, K. Mechanical and Functional Properties of a Novel Apatite-Ionomer Cement for Prevention and Remineralization of Dental Caries. *Materials* **2019**, *12*, 3998. [[CrossRef](#)]
19. Nakano, K.; Kubo, H.; Nakajima, M.; Honda, Y.; Hashimoto, Y. Bone Regeneration Using Rat-Derived Dedifferentiated Fat Cells Combined with Activated Platelet-Rich Plasma. *Materials* **2020**, *13*, 5097. [[CrossRef](#)]
20. Kim, H.W.; Kim, H.E.; Salih, V. Stimulation of osteoblast responses to biomimetic nanocomposites of gelatin-hydroxyapatite for tissue engineering scaffolds. *Biomaterials* **2005**, *26*, 5221–5230. [[CrossRef](#)]
21. Sharifi, E.; Ebrahimi-Barough, S.; Panahi, M.; Azami, M.; Ai, A.; Barabadi, Z.; Kajbafzadeh, A.M.; Ai, J. In vitro evaluation of human endometrial stem cell-derived osteoblast-like cells' behavior on gelatin/collagen/bioglass nanofibers' scaffolds. *J. Biomed. Mater. Res. A* **2016**, *104*, 2210–2219. [[CrossRef](#)]
22. Sasayama, S.; Hara, T.; Tanaka, T.; Honda, Y.; Baba, A.S. Osteogenesis of Multipotent Progenitor Cells using the Epigallocatechin Gallate-Modified Gelatin Sponge Scaffold in the Rat Congenital Cleft-Jaw Model. *Int. J. Mol. Sci.* **2018**, *19*, 3803. [[CrossRef](#)] [[PubMed](#)]
23. Yılmaz, P.; öztürk Er, E.; Bakırdere, S.; ülgen, K.; özbek, B. Application of supercritical gel drying method on fabrication of mechanically improved and biologically safe three-component scaffold composed of graphene oxide/chitosan/hydroxyapatite and characterization studies. *J. Mater. Res. Technol.* **2019**, *8*, 5201–5216. [[CrossRef](#)]
24. Kitamura, M.; Ohtsuki, C.; Ogata, S.-I.; Kamitakahara, M.; Tanihara, M.; Miyazaki, T. Mesoporous Calcium Phosphate Via Post-Treatment of alpha-TCP. *J. Am. Ceram. Soc.* **2005**, *88*, 822–826. [[CrossRef](#)]
25. Jeong, J.E.; Park, S.Y.; Shin, J.Y.; Seok, J.M.; Byun, J.H.; Oh, S.H.; Kim, W.D.; Lee, J.H.; Park, W.H.; Park, S.A. 3D Printing of Bone-Mimetic Scaffold Composed of Gelatin/beta-Tri-Calcium Phosphate for Bone Tissue Engineering. *Macromol. Biosci.* **2020**, *20*, e2000256. [[CrossRef](#)] [[PubMed](#)]
26. Li, J.; Chen, Y.; Yin, Y.; Yao, F.; Yao, K. Modulation of nano-hydroxyapatite size via formation on chitosan-gelatin network film in situ. *Biomaterials* **2007**, *28*, 781–790. [[CrossRef](#)]
27. Solchaga, L.A.; Tognana, E.; Penick, K.; Baskaran, H.; Goldberg, V.M.; Caplan, A.I.; Welter, J.F. A Rapid Seeding Technique for the Assembly of Large Cell Scaffold Composite Constructs. *Tissue Eng.* **2006**, *12*, 1852–1863. [[CrossRef](#)] [[PubMed](#)]
28. Wang, J.; Asou, Y.; Sekiya, I.; Sotome, S.; Orii, H.; Shinomiya, K. Enhancement of tissue engineered bone formation by a low pressure system improving cell seeding and medium perfusion into a porous scaffold. *Biomaterials* **2006**, *27*, 2738–2746. [[CrossRef](#)]
29. Yanagi, T.; Kajiya, H.; Fujisaki, S.; Maeshiba, M.; Yanagi, A.; Yamamoto, N.; Kakura, K.; Kido, H.; Ohno, J. Three-dimensional spheroids of dedifferentiated fat cells enhance bone regeneration. *Regen. Ther.* **2021**, *18*, 472–479. [[CrossRef](#)]
30. Watanabe, H.; Goto, S.; Kato, R.; Komiyama, S.; Nagaoka, Y.; Kazama, T.; Yamamoto, C.; Li, Y.; Konuma, N.; Hagikura, K.; et al. The neovascularization effect of dedifferentiated fat cells. *Sci. Rep.* **2020**, *10*, 9211. [[CrossRef](#)] [[PubMed](#)]
31. Kim, H.K.; Lee, S.G.; Lee, S.W.; Oh, B.J.; Kim, J.H.; Kim, J.A.; Lee, G.; Jang, J.D.; Joe, Y.A. A Subset of Paracrine Factors as Efficient Biomarkers for Predicting Vascular Regenerative Efficacy of Mesenchymal Stromal/Stem Cells. *Stem Cells* **2019**, *37*, 77–88. [[CrossRef](#)] [[PubMed](#)]